THE ASTROPHYSICAL JOURNAL, 325:927–938, 1988 February 15

ABUNDANCES IN COMET HALLEY AT THE TIME OF THE SPACECRAFT ENCOUNTERS[1]

SUSAN WYCKOFF, STEPHEN TEGLER, AND PETER A. WEHINGER
Department of Physics, Arizona State University
HYRON SPINRAD
Department of Astronomy, University of California–Berkeley
AND
MICHAEL J. S. BELTON
Kitt Peak National Observatory, National Optical Astronomy Observatories[2]
Received 1987 July 14; accepted 1987 August 13

ABSTRACT

Spectrophotometric observations of comet Halley were obtained in 1986 March at the time of the spacecraft encounters with the comet. Spatial profiles extracted from the long-slit spectra were analyzed to determine scale lengths for the observed radicals, C_2, NH_2, and CH, and their respective parent molecules. The surface brightness profile of NH_2 along the comet tail axis was well fitted by a simple point-source model with a two-step exponential decay. The C_2 and CH surface brightness distributions could not be fitted with the simple model. The scale length for the parent of NH_2 was found to be 1.1×10^4 km and that for NH_2, 1.6×10^4 km at $r = 1$ AU. Production rates for each of the observed neutral species were calculated using the vectorial model. For 1986 March 13.4 the ratio of production rates $Q(NH_2)/Q(H_2O) = 3 \times 10^{-3}$, indicates that $Q(NH_3)/Q(H_2O) \approx 0.3\%$ which is nearly 10 times lower than determined from *GIOTTO* ion mass spectrometer data. Our data indicate that the abundance of the primordial condensate, NH_3 comprises $\sim 0.2\%$ of the total volatile fraction of the comet nucleus. The production rate ratio, $Q(CH)/Q(H_2O) = 7 \times 10^{-3}$ and the CH spatial profile indicate that CH cannot derive entirely from direct photodissociation of CH_4. Rather the CH probably arises from multiple parents or a slowly sublimating source, such as the newly discovered CHON particles, or both.

Subject headings: abundances — comets

I. INTRODUCTION

Comets offer the best opportunity to determine the abundances of condensed primordial solar material as the cometary ices have undergone relatively little external or internal processing since formation. An especially favorable opportunity to determine the abundances of a comet nucleus occurred with the spacecraft *in situ* observations of comet Halley in 1986 March. The *VEGA* and *GIOTTO* spacecraft transited the Sunward side of the comet nucleus at distances of ~ 8000 km and ~ 600 km, respectively, and sampled the composition of the gas and dust components of the coma (Balsiger *et al.* 1986; Krankowsky *et al.* 1986; Kissel *et al.* 1986*a*, *b*). Both the spacecraft and *IUE* satellite data indicated a relatively large abundance, $\sim 10\%$–15% of CO relative to H_2O (Combes *et al.* 1986; Eberhardt *et al.* 1986; Woods, Feldman, and Dymond 1986). If the observed CO derives from the highly volatile condensate CO, then the large relative abundance of CO indicates that comet Halley probably formed at a distance very remote from the Sun, $r \gtrsim 100$ AU ($T \lesssim 25$ K). At present the sites of formation of comets are in some dispute (see, Spinrad 1987). Bailey (1986) has suggested that all short-period ($P \lesssim 200$ yr) comets condensed at the periphery of the solar accretion disk, in the Inner Oort Cloud, $r = 100$–$10{,}000$ AU. On the other hand, the long-period ($P \gtrsim 200$ yr) comets evidently now originate in the Oort Cloud, a reservoir of $\sim 10^{12}$ comet nuclei in loosely bound orbits $\sim 25{,}000$ AU from the Sun (Oort 1950). The current scenario is that long-period comet nuclei condensed from the solar accretion disk near $r \approx 20$–30 AU and were gravitationally scattered by Uranus and Neptune into the Oort Cloud (Fernandez 1978, 1985; Fernandez and Ip 1981, 1983) where the cometary orbits were subsequently randomized by galactic tides (Torbett 1986; Heisler and Tremaine 1986) and to a lesser extent by perturbations by random stars (Oort 1950) and giant molecular clouds (Thaddeus 1986; Scoville and Saunders 1986). As the orbit of comet Halley is atypical for a short-period comet (see Weissman 1985), the orbital characteristics do not yet provide clues to the comet's site of origin nor its subsequent evolution. The purpose of this paper is to study the chemical composition of comet Halley to gain insight into the conditions for formation and subsequent evolution of these low-mass solar system objects.

In § II we describe the observations and present in § III the column densities derived from the integrated emission band fluxes. The scale lengths are determined from the spatial profiles of the observed species in § IV. In § V we derive production rates, and in § VI we discuss the parent identities and abundance ratios of the species studied. Here we confine our study to the neutral radicals observed in comet Halley near the times of the spacecraft encounter missions.

II. OBSERVATIONS

Long-slit spectra of comet Halley were obtained with the 4 m Cerro Tololo Inter-American Observatory telescope on a photometrically clear night, 1986 March 13.4 UT, ~ 0.6 day

[1] Observations obtained at Cerro Tololo Inter-American Observatory, operated by the Association of Universities for Research in Astronomy, Inc., under contract with the National Science Foundation.

[2] Operated by the Association of Universities for Research in Astronomy, Inc., under contract with the National Science Foundation.

prior to the *GIOTTO* encounter and 4.4 days after the *VEGA 2* rendezvous with the comet. A photon-counting detector ("2D-FRUTTI") was used with the Cassegrain spectrograph and the Singer camera. The spectrograph slit, centered on the coma, was oriented in the direction of the extended solar radius vector, and had dimensions of 1 × 318″ on the plane of the sky. The spectral resolution at the detector was 4 Å, and the spatial resolution ~1.″5, with the spectra sampled at 2 Å pixel^{-1} in dispersion and at 0.″69 pixel^{-1} in the spatial direction. The spectral range covered 3950–7050 Å. At the time of the observations the heliocentric distance of the comet was $r = 0.88$ AU and the geocentric distance $\Delta = 0.99$ AU, which gave a spatial scale at the comet of 500 km arcsec^{-1}.

Data reduction was performed with NOAO's Image Reduction and Analysis Facility, IRAF, at Arizona State University. Comet Halley, the sky, and the standard star (LTT 4816) frames were corrected for the nonuniform instrumental sensitivity using a quartz lamp frame. The wavelengths were calibrated using He-Ne-Ar lamp frames, and the spatial calibration perpendicular to the direction of dispersion was done using a multihole aperture plate placed behind the spectrograph slit, through which the quartz lamp was exposed. Three integrations of Comet Halley with the slit centered on the nucleus and oriented along the tail axis were reduced. The three frames of the comet were separately extinction corrected using the CTIO mean extinction coefficients of Stone and Baldwin (1983). The Halley frames and the sky frame were flux calibrated using a sensitivity function obtained from the standard star LTT 4816 frame. Inspection of the individual two-dimensional Halley frames on a video monitor and assessment from preliminary reductions of the small dispersion in the measured band and band sequence fluxes, ~3%–5%, indicated that the three Halley frames could be summed to increase the signal-to-noise ratio. The extinction corrected comet frames were summed and then flux calibrated producing a frame corresponding to a 3205 s integration time. The flux-calibrated sky frame was then subtracted from the fluxed Halley frame. The sky integration was obtained at a position several degrees in the Sunward direction from the comet nucleus. Only the night sky emission features contributed significantly to the comet spectrum, and the background sky continuum was negligibly small. On 1986 March 13 the coma extended several tens of arcminutes on the sky.

One-dimensional extractions, both parallel(*w*-axis) and perpendicular(*s*-axis) to the spectral dispersion direction, were made from the sky-subtracted 3205 s Halley frame. The reduced frame was $W = 1500$ pixels in length and $S = 460$ pixels wide. A spectral extraction then represented a part of the frame W pixels long and Δs pixels wide. The Δs pixels were summed along the frame section to produce the spectrum. Spectral extractions with widths $\Delta s = 4$ and $\Delta s = 50$ pixels, corresponding to 2.″7 and 35″ apertures, respectively, were obtained from the summed Halley frame. The larger aperture spectrum was centered on the center of brightness of the coma, and the smaller aperture spectral extraction was offset in the tailward direction ~7 pixels (5000 km) from the center of brightness of the coma. Continuum radiation produced by solar photons scattered from the cometary dust was removed from the spectral extractions by fitting a reddened solar continuum to the cometary continuum. Integrated band and band sequence fluxes were obtained from each spectral extraction for the CN($\Delta v = -1$), CH(0–0), $C_2(\Delta v = +1)$, $C_2(\Delta v = 0)$, $C_2(\Delta v = -1)$, NH_2(10–0) emission features by numerical integration. Table 1 gives integrated fluxes obtained for both spectral extractions of the summed frame of comet Halley. The errors listed in Table 1 are determined by the uncertainties in fitting a reddened solar continuum to the extracted spectra. Figure 1 shows a spectrum from which the fluxes in column (4) of Table 1 were derived. The C_3 band near 4050 Å was not measured due to incomplete spectral coverage caused by the detector limit.

Orthogonal extractions in the spatial direction (along the *s*-axis) from the two-dimensional data provide surface brightness distributions of the flux emitted from CH(0–0), $C_2(\Delta v = 0)$, and NH_2(10–0). Prior to extracting a spatial profile of a molecular band or band sequence the background solar continuum was subtracted. This subtraction was done with a continuum spatial profile adjacent to the molecular band profile. Figure 2, for example shows a plot of the $C_2(\Delta v = 0)$ band sequence with the continuum contribution removed. The X-axis is the spatial dimension, the Y-axis is the wavelength dimension, and the vertical axis is flux. The continuum-subtracted spatial profiles of the molecular emission features were then obtained by extracting a section from the Halley frame, $\Delta w \times S$ pixels, where Δw corresponds to the wavelength interval of the molecular band or band sequence and S extended the full length of the frame, 460 pixels, corresponding to 2.3×10^5 km at the comet. Figures 3, 4, and 5 show the solar continuum-subtracted surface brightness profiles along the comet tail axis for the radicals CH(0–0), $C_2(\Delta v = 0)$, and NH_2(10–0).

TABLE 1

OBSERVED FLUXES

Molecule (1)	Band (2)	λ (Å) (3)	F^b (ergs cm^{-2} s^{-1}) (4)	F^c (ergs cm^{-2} s^{-1}) (5)
CN	$\Delta v = -1$	4216	$(3.4 \pm 0.7) \times 10^{-12}$	$(3.2 \pm 0.7) \times 10^{-13}$
C_2	$\Delta v = +1$	4737	$(5.9 \pm 0.8) \times 10^{-11}$	$(4.8 \pm 0.3) \times 10^{-12}$
	$\Delta v = 0$	5165	$(1.20 \pm 0.05) \times 10^{-10}$	$(1.01 \pm 0.02) \times 10^{-11}$
	$\Delta v = -1$	5635	$(6.4 \pm 0.6) \times 10^{-11}$	$(5.5 \pm 0.3) \times 10^{-12}$
NH_2	(10–0)	5730	$(5.5 \pm 1.1) \times 10^{-12}$	$(4.0 \pm 0.9) \times 10^{-13}$
CH	(0–0)	4315	$(6.7 \pm 1.9) \times 10^{-12}$	$(4.0 \pm 0.7) \times 10^{-13}$

[a] $r = 0.89$ AU.
[b] Aperture = 1 × 35″ = 720 × 25,000 km, centered on nucleus.
[c] Aperture = 1 × 2.″7 = 720 × 2000 km, centered 5000 km tailward.

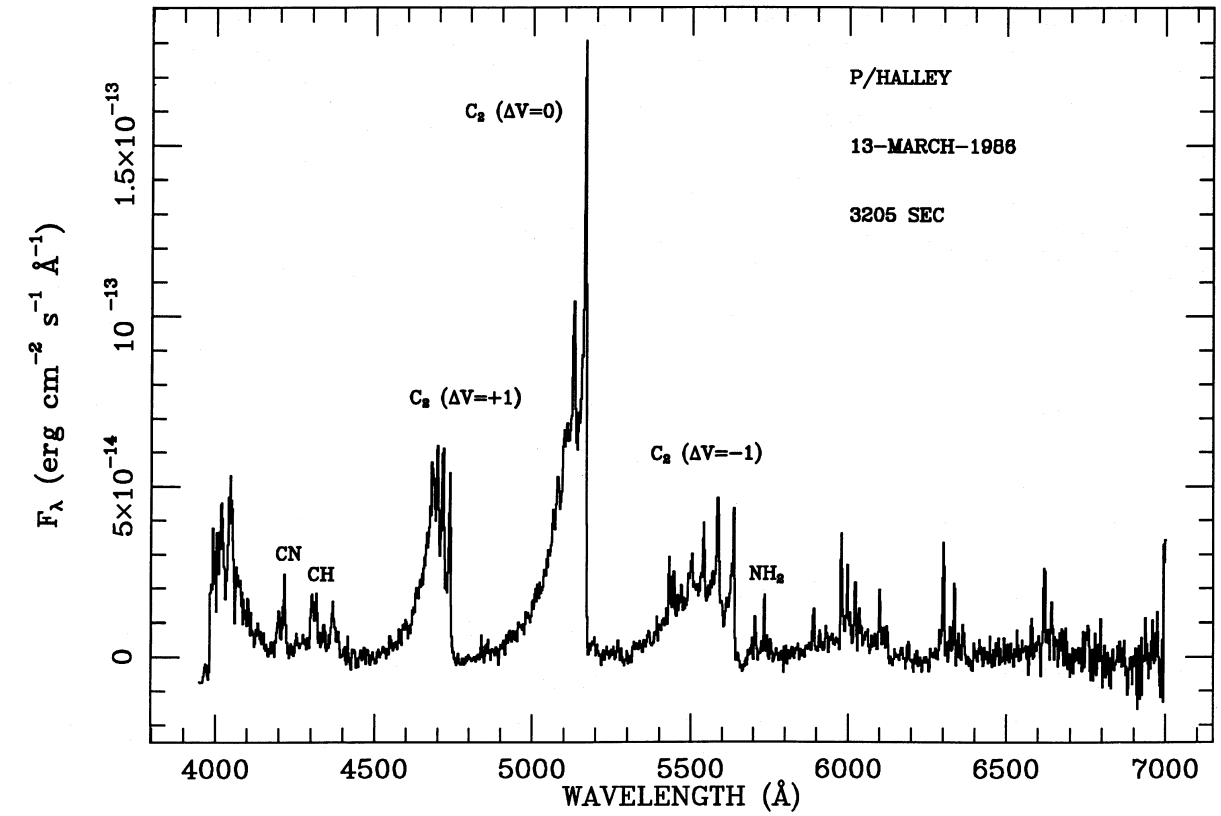

FIG. 1.—One dimensional extraction of the spectrum of comet P/Halley from a long-slit CCD frame. The extraction aperture was 1 × 35″ centered on the nucleus. Prominent spectral features are identified and their integrated fluxes and column densities are given in Tables 1 and 2. The spectrum was obtained 4.4 days after the *VEGA 2* spacecraft encounter and ~0.6 day prior to the *GIOTTO* encounter.

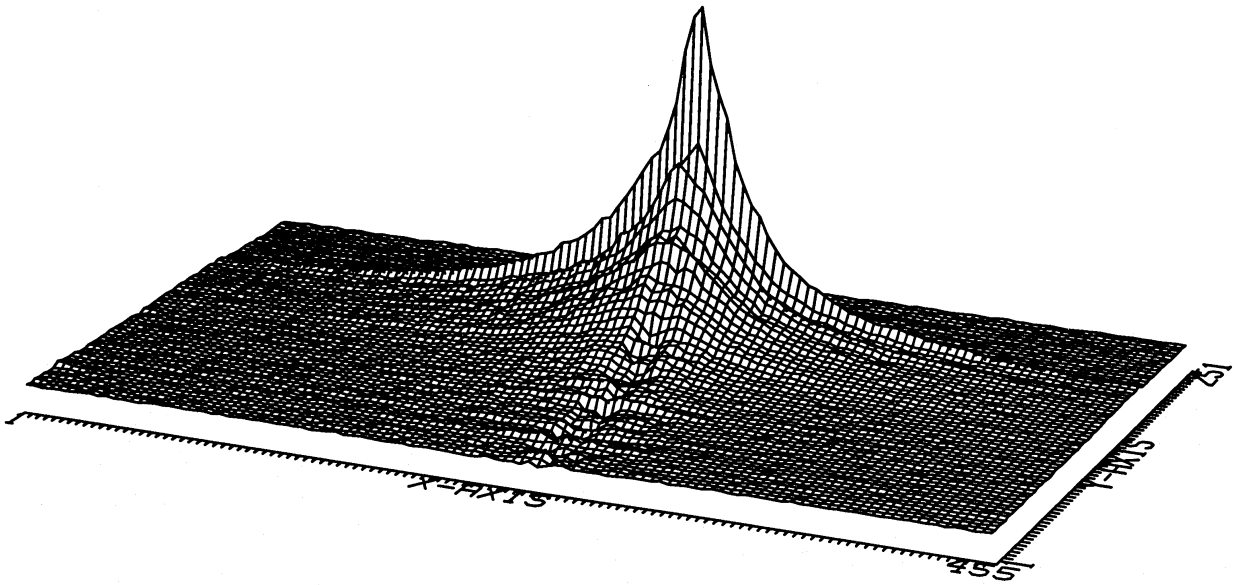

FIG. 2.—Spatially resolved profile of C_2 5165 Å band of comet Halley where surface brightness of the emission band after subtraction of the background dust continuum is displayed. Units are in CCD pixels where the *X*-axis represents the spatial direction along the tail axis (solar direction to the right), and the *Y*-axis is parallel to the spectrum dispersion with increasing wavelength upward and to the right. The peak C_2 intensity is given in Fig. 1 and the scales correspond to 500 km pixel^{-1} (*X*-axis) and 2 Å pixel^{-1} (*Y*-axis).

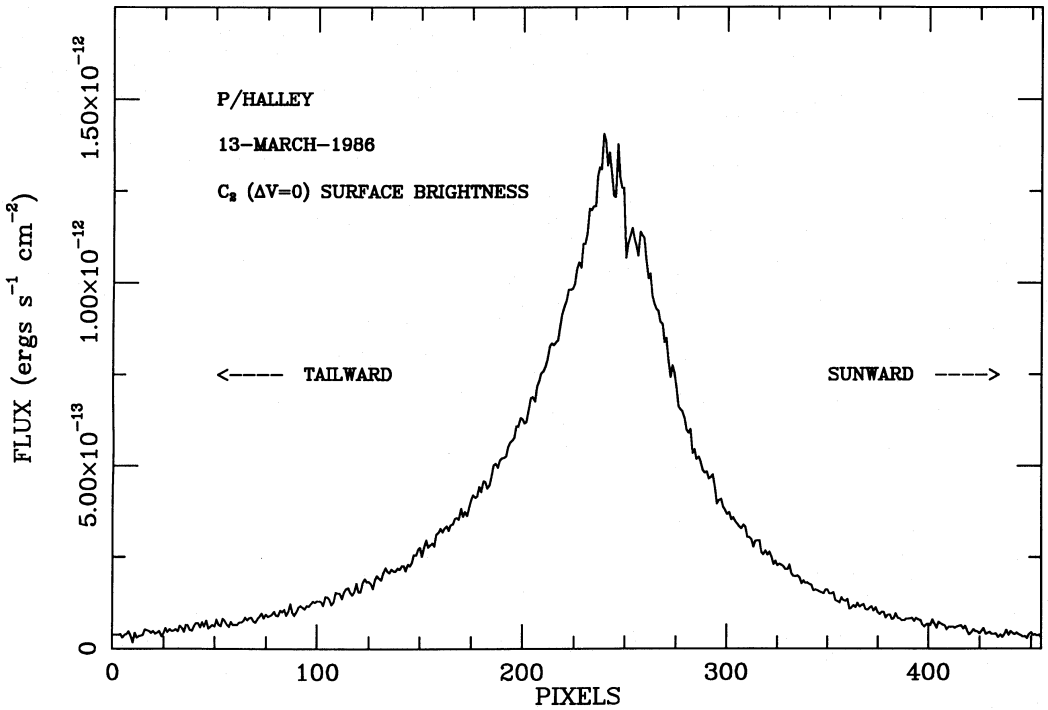

FIG. 3.—Surface brightness profile of C_2 at 5165 Å summed over the $\Delta v = 0$ band sequence and projected along the comet tail axis. The adjacent dust continuum was subtracted from the emission band prior to extraction of the spatial profile. (One pixel corresponds to 500 km at the comet in Figs. 3–5 and Fig. 9.)

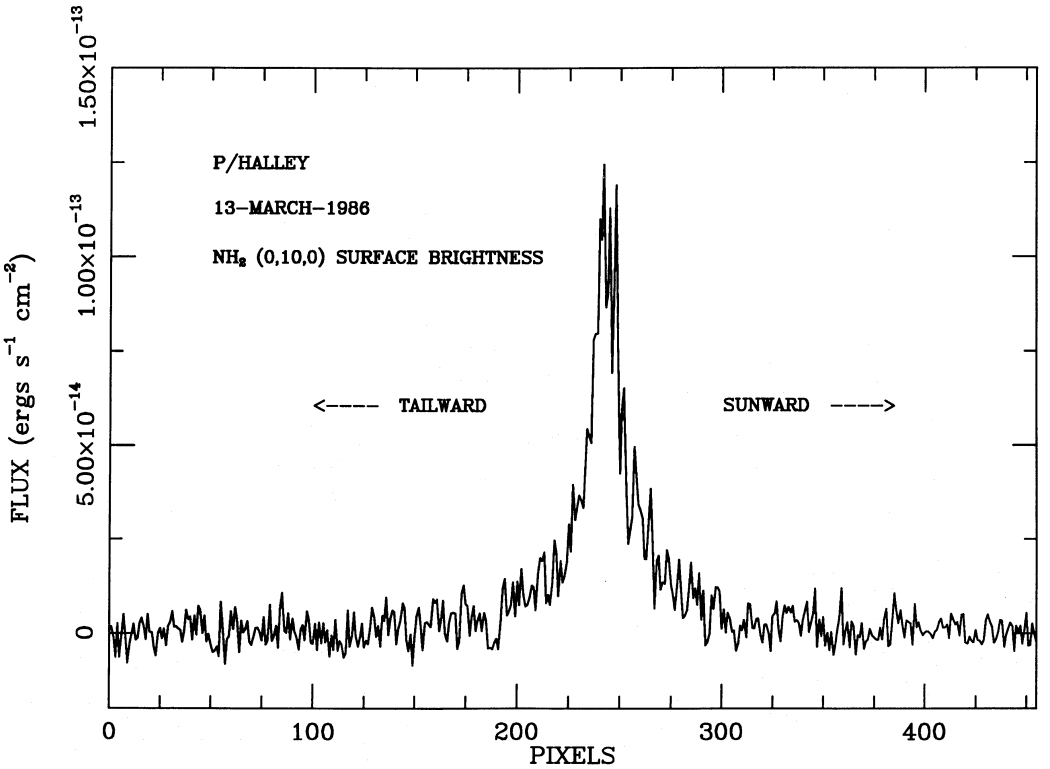

FIG. 4.—Surface brightness profile of the NH_2 (10–0) band (5730 Å) with adjacent dust continuum subtracted. Note the relatively short extent and steepness of the NH_2 profile, indicative of short parent and NH_2 scale lengths.

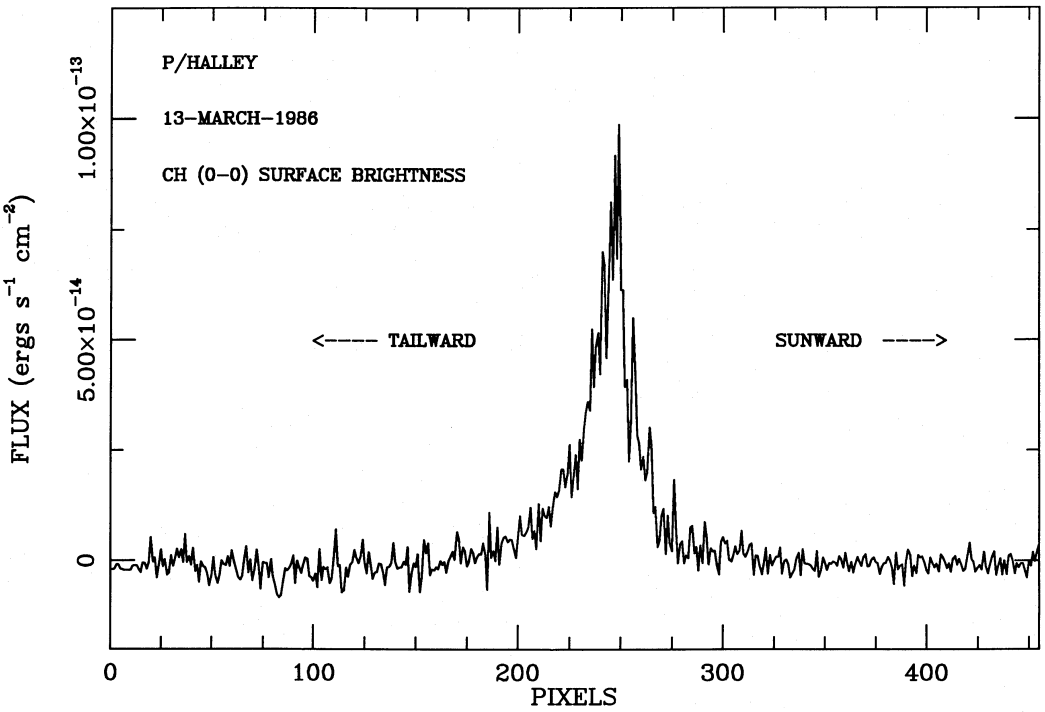

FIG. 5.—Surface brightness profile of the CH (0–0) band (4315 Å) with adjacent dust continuum subtracted

III. COLUMN DENSITIES

The fluorescence efficiencies or g-factors relate the flux measurements to column densities. In particular,

$$N = \frac{4\pi F}{\Omega g}, \tag{1}$$

where N is the column density of a given species, Ω is the solid angle subtended by the observing aperture at the comet, determined by the size of the spectral extraction, F is the integrated molecular band strength, and g is the efficiency for fluorescent scattering (see Chamberlain and Hunten 1987) which for a molecular band is

$$g_{v'v''} = \frac{\pi F_{\odot}(\pi e^2)\lambda^2_{v'v''} f_{v'v''} A_{v'v''}}{r^2 mc^2 \sum_{v''} A_{v'v''}}, \tag{2}$$

where $\pi F_{\odot}$ is the solar irradiance at a heliocentric distance, r(AU), in photons cm^{-2} s^{-1} Å^{-1}, $\lambda_{v'v''}$ is the wavelength of the molecular band in Å, $f_{v'v''}$ is the band oscillator strength, and $A_{v'v''}/\sum A_{v'v''}$ is the branching ratio for transitions into the lower level of the observed transition. For the above units the constant $(\pi e^2/mc^2) = 8.85 \times 10^{21}$ cm Å^{-1}. Although the Swings effect (Swings 1941) determined by absorption lines in the solar spectrum can affect the fluorescence efficiency, the g-factors for all species except CN were calculated from an average of the solar irradiance over the individual molecular band or band sequence intervals (A'Hearn 1982). For a heliocentric radial velocity ~ 0 km s^{-1} the cometary CH fluorescence would be most affected by the Swings effect, because the G-band is a relatively strong feature in the solar Fraunhofer spectrum. However, on 1986 March 13.4 the heliocentric radial velocity of the comet ($\sim +25$ km s^{-1}) shifted the cometary CH molecules out of the solar CH flux minima. The error committed in ignoring the Swings effect in calculating the g-factors for the observed molecular bands is estimated to be $\leq 5\%$ much less than the error in the integrated fluxes. The g-factor for the CN($\Delta v = -1$) sequence was taken from Schleicher (1981) who took account of the Swings effect. The g-factors adopted and calculated column densities are given in Table 2, where the internal errors are in the range $\sim 2\%$–20%. We estimate the errors in the absolute calibration of the fluxes to be $\sim 15\%$.

IV. SCALE LENGTHS

In order to determine the production rates of the various species observed in comet Halley from the observed column densities, scalelengths for the radicals and their parents must be determined. The long-slit spectra are particularly well-suited for determining these scale lengths, since both the scale length and column densities can be obtained from the same data. For comet Halley the observed H_2O production rate was varying by a factor of 2 or 3 from day to day in 1986 March (Feldman *et al.* 1986; Mumma, Weaver, and Larson 1986), so the contemperaneous determination of the scale lengths and column densities may be essential for accurate calculation of the production rates. The surface brightness profiles extracted from the spectra (Figures 3, 4, and 5) were modeled to derive scale lengths. The relatively weak CN (1–0) band observed at 4216 Å did not have a well-determined spatial profile. The strong CN (0–0) band of the violet system was deliberately placed outside the observed wavelength range, as the dynamic range of the detector was insufficient to record both the CN (0–0) band and the other much weaker cometary emission fea-

TABLE 2

FLUORESCENCE EFFICIENCIES AND OBSERVED COLUMN DENSITIES

Molecule	g[a] (photons s^{-1})	λ (Å)	M[b] (molecule) $\times 10^{29}$	N[b] (molecule cm^{-2}) $\times 10^{12}$	M[c] (molecule) $\times 10^{28}$	N[c] (molecule cm^{-2}) $\times 10^{12}$
CN	0.0055	4216	2.9 ± 1.5	1.6 ± 0.8	2.7 ± 0.6	1.8 ± 0.4
C_2	0.053	4737	5.7 ± 0.8	3.2 ± 0.4	4.7 ± 0.3	3.2 ± 0.2
	0.116	5165	5.8 ± 0.2	3.3 ± 0.1	4.9 ± 0.1	3.3 ± 0.1
	0.069	5635	5.7 ± 0.5	3.2 ± 0.3	4.9 ± 0.3	3.3 ± 0.2
NH_2	0.0087	5730	4.0 ± 0.8	2.3 ± 0.5	2.9 ± 0.7	2.0 ± 0.5
CH	0.020	4315	1.6 ± 0.4	0.9 ± 0.3	1.0 ± 0.2	0.6 ± 0.1

[a] For $r = 1$ AU.
[b] Aperture = $1 \times 35'' = 720 \times 25{,}000$ km, centered on nucleus, $r = 0.89$ AU.
[c] Aperture = $1 \times 2''.7 = 720 \times 1940$ km, centered 5000 km tailward from nucleus, $r = 0.89$ AU.

tures. Thus the scale length for CN and its parent were taken from the literature (see references in Table 3).

The density distribution of an observed molecular species, $n(R)$, as a function of radial distance from the comet nucleus, R, can be represented by a two-step photodissociation decay process (Haser 1957),

$$n(R) = \left(\frac{Q}{4\pi R^2 v}\right)\left(\frac{\beta_p}{\beta_d - \beta_p}\right)(e^{-\beta_p R} - e^{\beta_d R}) , \quad (3)$$

where Q is the production rate of the species, v is the parent molecule outflow velocity, β_p is the reciprocal of the parent molecule scalelength, and β_d is the reciprocal of the observed (daughter) species scalelength.

The outflow velocity of the parent molecule as a function of heliocentric distance is given by (see Delsemme 1982),

$$v = v_0 r^{-0.5} . \quad (4)$$

For many years the outflow velocity $v_0 \approx 0.58$ km s^{-1} at $r = 1$ AU obtained from photographic observations of structure in the coma, has been used in modeling coma outflows (see Delsemme 1982). Recently, however, direct Doppler velocity measurements of the expanding coma of comet Halley were measured. Two different parent molecules were measured. Schloerb *et al.* (1986) used radio line measurements of HCN to measure $v_0 = 1.0$ km s^{-1} in mid-March of 1986, and Larson *et al.* (1986) measured an outflow velocity for H_2O from the infrared line widths on 1986 March 22, $v_0 = 1.4 \pm 0.2$ km s^{-1}. In addition, the ram energy spectrum of H_2O molecules measured by the neutral mass spectrometer experiment abroad the *GIOTTO* spacecraft gave an outflow velocity at $R \approx 2 \times 10^4$ km, $v_0 \approx 1.0 \pm 0.5$ km s^{-1} (Eberhardt *et al.* 1986). Here we adopt a parent outflow velocity, $v_0 = 1$ km s^{-1}. For the photodissociation (daughter) products which were observed, velocities were calculated assuming that the energy excess from the photodissociation process was entirely converted, with momentum conserved, to the kinetic energies of the daughter molecules. These velocities provided checks on the destruction timescales of parent and daughter molecules.

TABLE 3

ADOPTED SCALE LENGTHS[a]

Molecule	β_p^{-1} (km)	β_d^{-1} (km)
CN[b]	1.6×10^4	3.3×10^5
C_2	3.2×10^4	1.0×10^5
NH_2	1.1×10^4	1.6×10^4
CH	1.2×10^5	6.0×10^3

[a] $r = 1$ AU.
[b] See Newburn and Spinrad 1984; Cochran 1985, 1987; Bockelée-Morvan and Crovisier 1985; Combi and Delsemme 1986; Schloerb *et al.* 1986.

The Haser model was used to determine the scale lengths for C_2, NH_2, and CH and their respective parent molecules. Since we observe the projection of the comet coma on the plane of the sky, the observed column density at projected distance ρ from the nucleus, for a given species was obtained by integrating equation (3) along the line of sight (see O'Dell and Osterbrock 1962),

$$N(\rho) = CS(\rho) = \frac{C}{\beta_d \rho}\left[B(\beta_d \rho) - B(\beta_p \rho)\right] , \quad (5)$$

where

$$B(z) = \frac{\pi}{2} - \int_0^z K_0(y)dy , \quad (6)$$

and $K_0(y)$ is the modified Bessel function of zero order and the second kind, C is a constant with units determined by $S(\rho)$, the observed surface brightness. To determine the inverse scale lengths, β_p and β_d, for each species we used a best-fit procedure.

Since the spatial information is limited by both the slit length and the spatial resolution of the instrument, the scale lengths determined using the Haser model are reliable only if two constraints are fulfilled, namely that the species' scalelengths are (1) shorter than the projected slit length, yet (2) longer than the spatial resolution. The ratio of the projected observing aperture (slit length in this case), $S \approx 2.3 \times 10^5$ km, to the species scale length is $\gamma = S/(\beta_p^{-1} + \beta_d^{-1})$. For $\gamma > 1$ the projected slit length has sufficient extension for determining reliable Haser scalelengths. The second constraint is the spectral spatial resolution, θ, which sets the lower limit for scalelength determinations. For a comet geocentric distance, Δ, the condition for resolving a species' scalelength is $\kappa = [(\beta_p^{-1} + \beta_d^{-1})/\theta\Delta] > 1$, where $\theta \approx 10^{-5}$ rad for our CTIO spectra and $\Delta = 0.99$ AU. Thus for those molecular emission features with sufficient signal-to-noise ratio after subtraction of the background dust continuum, scalelengths could be well determined if the parameters γ and $\kappa > 1$. For the present observations, $C_2(\gamma \approx 2, \kappa \approx 180)$, $NH_2(\gamma \approx 8, \kappa \approx 37)$ and $CH(\gamma \approx 2, \kappa \approx 173)$ all have expected scale lengths within the instrumental spatial limit constraints. However, for CN, $\gamma \approx 1$, so that the scale length is comparable to the projected instrument slit length, which is another reason that we have adopted CN scale lengths from other sources.

The Sunward and tailward logarithmic surface brightness profiles of C_2, NH_2, and CH are shown in Figures 6, 7, and 8, respectively, together with the best-fit Haser models. The corresponding scale lengths are discussed below and summarized in Table 3. The error bars in the surface brightness profiles (Figs. 6–8) represent photon counting statistics, and range from a few percent to 15% depending on the strengths of the emission features and the projected distance from the comet nucleus. The references given in Table 3 are for sources from which the adopted CN scale lengths were derived. The C_2 scale lengths obtained here agree well with previous determinations for other comets (see A'Hearn 1982; Cochran 1985, 1987*b*; Newburn and Spinrad 1984). The fit of the Haser model to the C_2 profile, however, could not be improved beyond that in Figure 6. We note in particular the flatness of the observed C_2 profile near the nucleus. Random seeing effects and telescope tracking errors would tend to flatten the spatial profiles of all species near the nucleus by the same amount. We estimate our tracking error to be $\lesssim \pm 1000$ km. Intercomparison of the spatial profiles for C_2 and NH_2 (Figs. 6 and 7) demonstrates that the flatness of the observed C_2 distribution cannot be attributable to random seeing or telescope tracking errors. Also, the symmetry of the Sunward and tailward profiles indicates that systematic tracking errors parallel to the slit entrance aperture are insignificant. It is noteworthy that the C_2 spatial profiles observed in several comets by Cochran (1985) also appear to flatten compared to Haser models near the nucleus ($\lesssim 10^4$ km). We conclude that the Haser model only fairly approximates the C_2 distribution, and we suggest that (1) more than one parent or (2) a distributed source, or both, may be needed to at least partially explain the C_2 origin in comets as has been previously suggested (Newburn and Spinrad 1984; A'Hearn *et al.* 1986*b*).

Few reliable determinations of the CH or the NH_2 scale lengths have previously been reported, as both generally have weak spectral features with relatively small spatial extents. Our results indicate a relatively short scale length for NH_2, in basic agreement with Delsemme and Combi (1983) for comet Kohoutek. As can be seen from the fit of the Haser scale lengths to the spatial profile in Figure 7, NH_2 is well approximated by the model. We interpret this fit to mean that the two-step decay process is a good model for NH_2, and also that the assumption of a single point source parent is accurate for NH_2.

The spatial extent of CH in the coma of comet Halley is somewhat puzzling. The observed CH profile in Figure 8 is compared with two Haser models. The best fit to the observations is that model in which both the parent and daughter molecule scale lengths were free parameters (*solid line*). The other model shown in Figure 8 is the Haser model best-fit which was constrained by the CH photodissociation rate (*dot-dashed* line). Recent calculations show that predissociation from the $C^2\Sigma^+$ state controls the dissociation of CH by solar radiation (Gredel 1987; Singh and Dalgarno 1987). For $r = 0.89$ AU and $\dot{r} = +25.5$ km s^{-1} the photodissociation lifetime for CH is $\tau = 300$ s. Thus for an assumed CH outflow velocity, $v \approx 2$ km s^{-1}, we calculate a scale length, $\beta_d^{-1} = v\tau = 600$ s. The Haser model constrained by this calculated photodissociation scale length clearly does not fit the observed CH profile as well as the other model shown in Figure 8 for

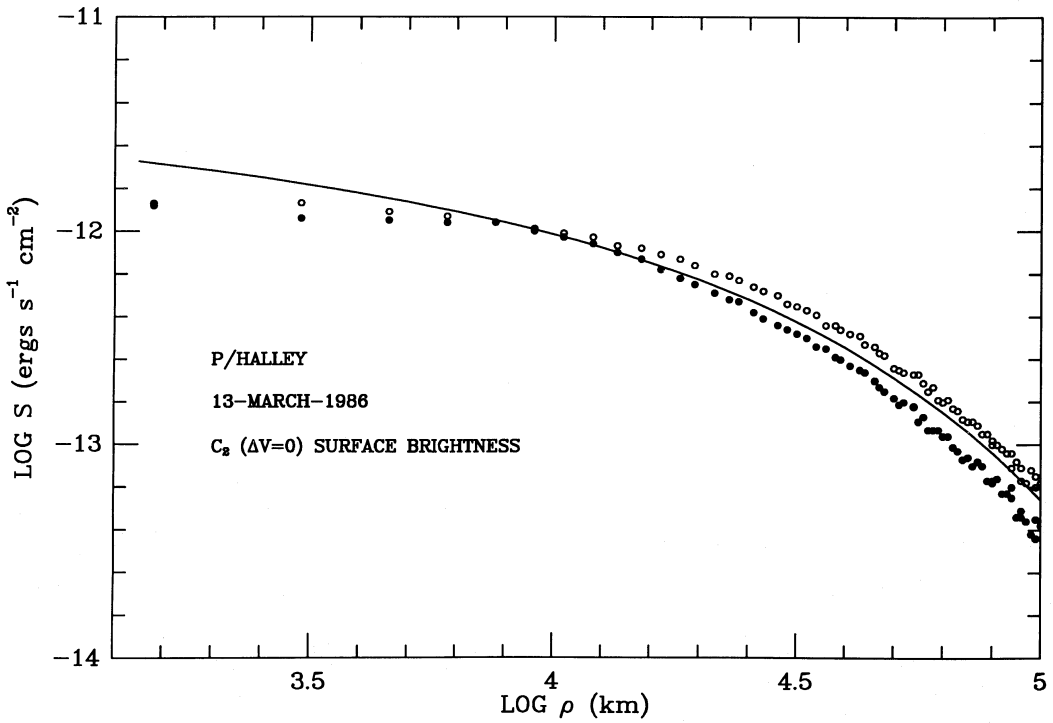

FIG. 6.—Logarithmic plot of tailward (*open circles*) and Sunward (*filled circles*) C_2 surface brightness vs. projected distance from the nucleus, ρ. Best-fit Haser model is indicated (*solid line*) scale lengths given in Table 3. Note the flatness of the observed profile relative to the model near the nucleus.

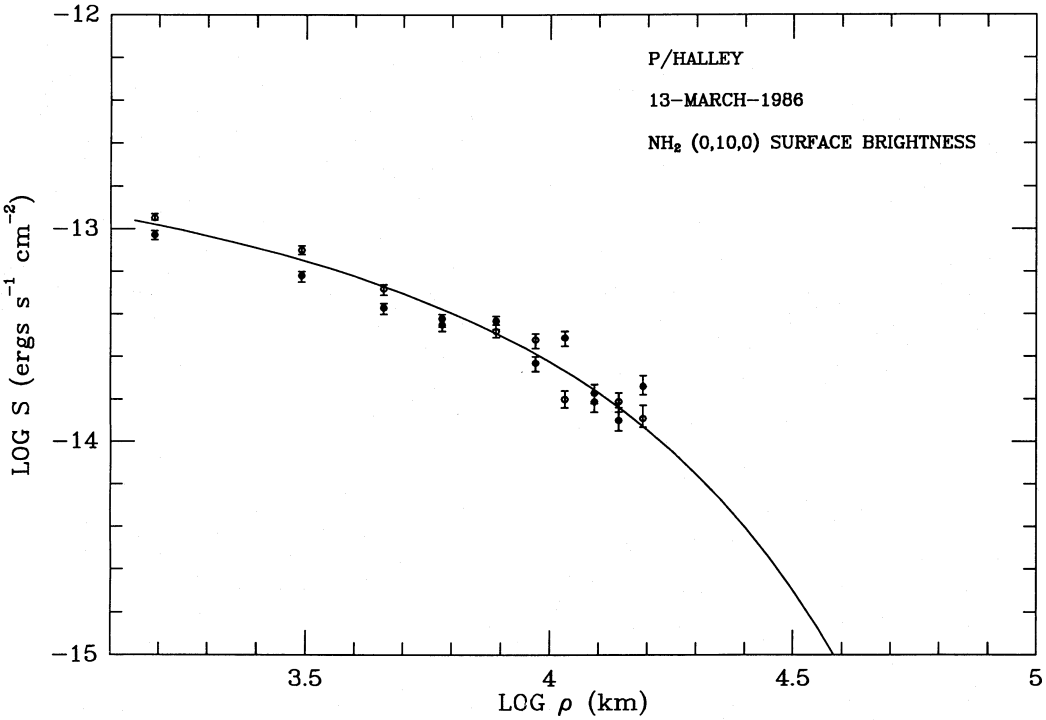

FIG. 7.—Logarithmic plot of tailward (*open circles*) and Sunward (*filled circles*) NH_2 surface brightness profiles which illustrates a good fit of the Haser model (*solid line*). The quality of the fit indicates that the point source two-step decay model approximates the NH_2 profile quite well.

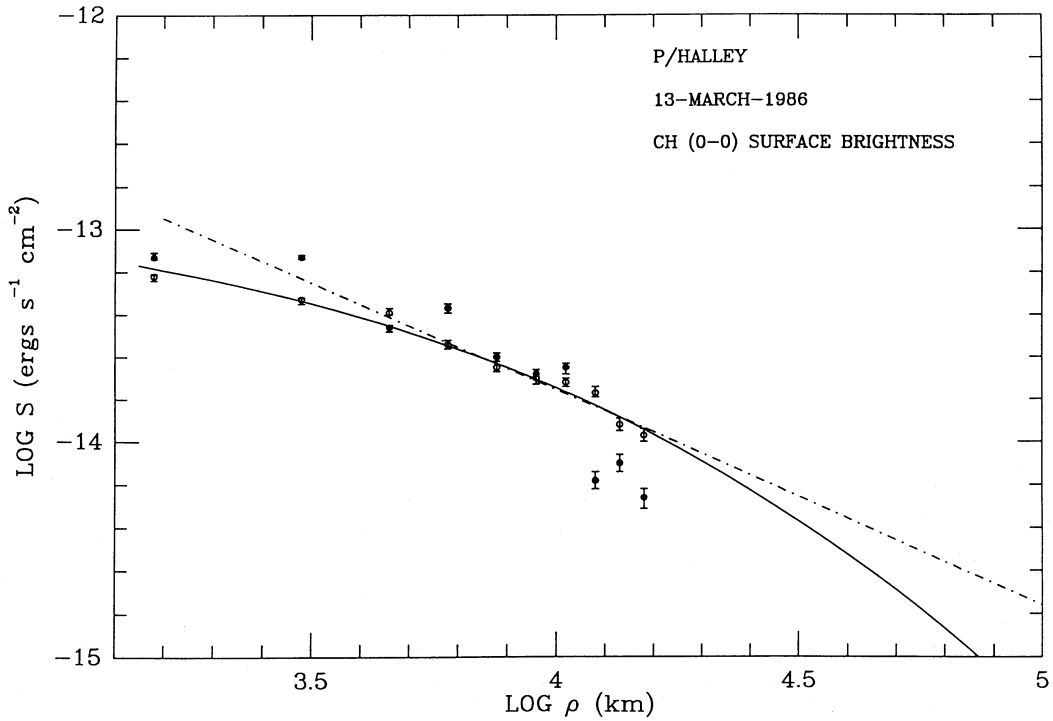

FIG. 8.—Logarithmic plot of tailward (*open circles*) and Sunward (*filled circles*) CH surface brightness profiles. The best-fit Haser model with parent and daughter scale lengths as free parameters (*solid line*) and the best-fit constrained by the CH photodissociation rate (*dot-dashed line*) are indicated.

TABLE 4

PRODUCTION RATES—1986 MARCH 13.4

X_i	$Q(X_i)$ (molecules s^{-1})	$Q(X_i)/Q(H_2O)$[a]
CN	$(1.0 \pm 0.3) \times 10^{27}$	0.002
C_2	$(2.7 \pm 0.2) \times 10^{27}$	0.004
NH_2	$(1.6 \pm 0.3) \times 10^{27}$	0.003
CH	$(4.1 \pm 1.2) \times 10^{27}$	0.007

[a] $r = 0.89$ AU.

[b] $Q(H_2O) = 6 \times 10^{29}$ molecules s^{-1}; Feldman *et al.* 1986.

which the scale lengths are given in Table 4. We conclude from Figure 8 that a scale length significantly longer than the calculated CH photodissociation scale length is required to fit the data using the Haser model. Thus the simple two-step decay point source model approximates NH_2 better than CH, and we attribute the failure of the Haser model to fit the CH spatial profile to limitations of the model. Cochran (1987) has previously found the Haser model inadequate in accounting for the CH distribution in comet comae.

The long parent lifetime for CH inferred from Figure 8 may indicate an origin in a slowly volatilizing component of the coma, as has been suggested for the parents of C_2 and CN (A'Hearn *et al.* 1986*a*). In fact, the CHON particles discovered by the spacecraft dust analyzers (see Kissel *et al.* 1986*a*, *b*) would be the most likely source of CH. If the CHON particles are the sources of C_2, CN, and CH, then the parent scale lengths of these species would be comparable if determined by a common, hypothesized low volatile material ("glue") (Houpis and Gombosi 1986). However, we have found that the parent scale lengths of these three species differ by one order of magnitude (Table 3). One explanation for the observed scale lengths of the parent molecules of CN, C_2, and CH then is that these radicals are released from the dust or CHON particles and subsequently photodissociated on different time scales. This scenario for the parent molecules would indicate that they originated in a region distributed about the nucleus, rather than coming directly from the nucleus. Therefore a distributed source could account for the failure of the point-source Haser model to fit the flat portion of the C_2 surface brightness profile (Fig. 6) and give rise to the long parent scale length found for CH. Thus our observations of CH and C_2 provide evidence that the parents of CH and C_2 may arise in a slowly volatilizing, distributed source. The scale lengths given in Table 3 have been adopted as best estimates for the purpose of calculating the production rates discussed below.

Figure 9 shows the surface brightness profile of the dust continuum extracted from the two-dimensional spectrum at 5800 ± 10 Å. The profile shows a distinct Sunward asymmetry and a Sunward shift of the profile peak, not evident in the gas profiles extracted from the same spectrum (Figs. 3–5). We note that the dust profile in Figure 9 must arise from particles larger than the CHON particles which have sizes too small to scatter visible light. Both the asymmetry and the shift in the peak of the dust profile relative to the gas profiles can be explained by the finite gas molecule lifetimes and the relatively long dust lifetimes combined with the Sunward sublimation of the gas which drags the dust outward (Delsemme and Combi 1983).

The Sunward asymmetric distribution of the dust particles represented in Figure 9 was also observed in the *GIOTTO* and *VEGA* images where the dust appeared to be ejected Sunward

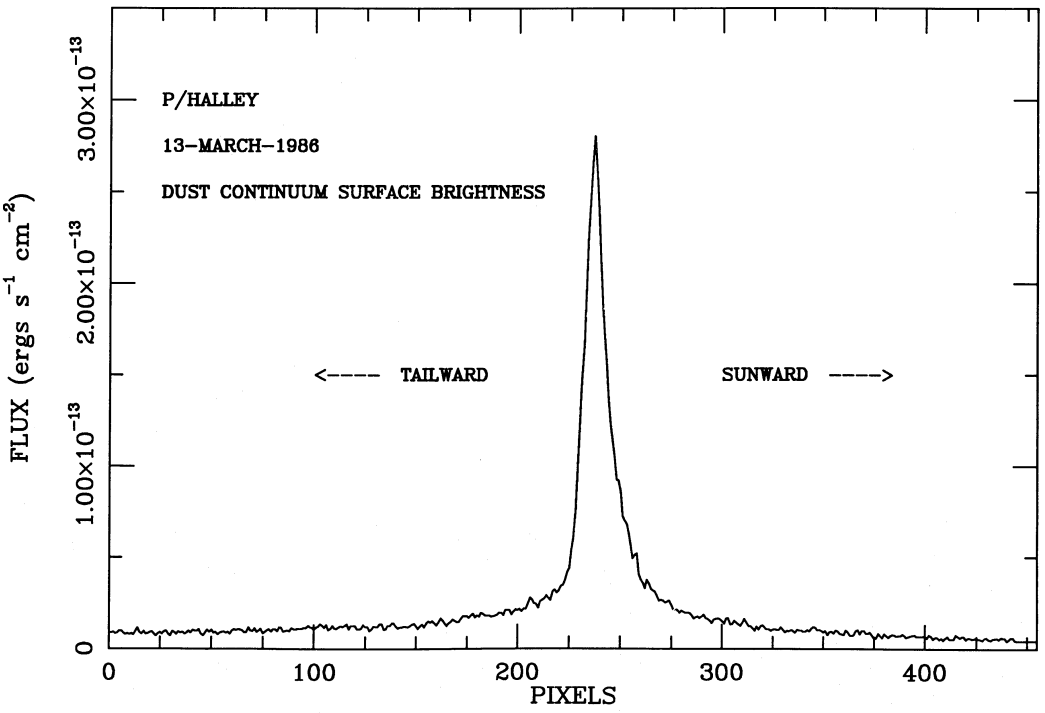

FIG. 9.—Spatial profile showing the Sunward asymmetry of the dust distribution. The peak intensity is shifted Sunward relative to the peaks of the gas profiles (Figs. 3–5) by ~5000 km.

in jets localized on a few percent of the Sunward-facing surface of the comet nucleus.

A Sunward asymmetry of the dust was also observed at virtually the same time as our observations in the infrared by Hayward, Gehrz, and Grasdalen (1987). Thus the Sunward ejection of dust which must map the dominant gas flow from the nucleus seems well-established by a variety of Halley observations.

The logarithmic surface brightness profiles of the Sunward and tailward dust profiles are shown in Figure 10 where a calculated ρ^{-1} surface brightness profile is displayed assuming a $n(R) \propto R^{-2}$ dependence of the dust volume density. The calculated profile fits the slope of the Sunward profile quite well, but does not account for the wave structure (scale length ~ 7000 km) evident in the observed tailward profile and probably present with a smaller amplitude in the Sunward profile. The error bars from the photon-counting statistics in Figure 10 are smaller than the plotting symbols; hence the wave structure is real, and requires a model for the dust distribution more complex than the spherical, uniform expansion model assumed here.

V. PRODUCTION RATES

The fluorescence efficiencies in Table 2 (A'Hearn 1982) and the adopted scale lengths in Table 3 were used to calculate production rates using a vectorial model (Festou 1981) for the gas outflow from the comet nucleus. Unlike the standard Haser model, Festou's (1981) model takes into account the isotropic velocity component acquired by the daughter molecule fragments in the photodissociation process and can therefore be considered an improvement over the Haser model. Scale lengths derived from fits to the surface brightness profiles by the Haser model in § IV were used as input parameters to the vectorial model. The errors quoted for the production rates reflect the uncertainties in the scale lengths as well as differences between models (Haser and vectorial), and observers. Cochran and Barker (1986) determined production rates for C_2 and CN from spectra of comet Halley obtained also on 1986 March 13. For the same assumed outflow velocities, our production rates agree within 30% with those derived by Cochran and Barker (1986). For each species the average column density at a projected distance ~ 5000 km from the nucleus on the tailward side of the coma was used to determine the final production rate. At this projected distance radiation pressure effects on the spatial profiles of all observed species are negligible. The results of the vectorial model calculations are given in Table 4 together with the estimated uncertainties.

The water production rate for comet Halley on 1986 March 13 was measured from OH (3080 Å) band emission strength by Feldman *et al.* (1986), $Q(H_2O) = 6 \times 10^{29}$ molecules s^{-1}, using the *IUE* satellite. The ratios of the production rates of the observed species, X_i, with water $Q(X_i)/Q(H_2O)$, are also given in Table 4.

The results in Table 4 indicate that the neutral radicals observed in the visible spectrum comprised $\sim 1\%$ of the gas component in comet Halley (Wegmann *et al.* 1987). Hence the most prominent spectral features in the comet coma (4000–7000 Å) represent trace constituents. The opposite is

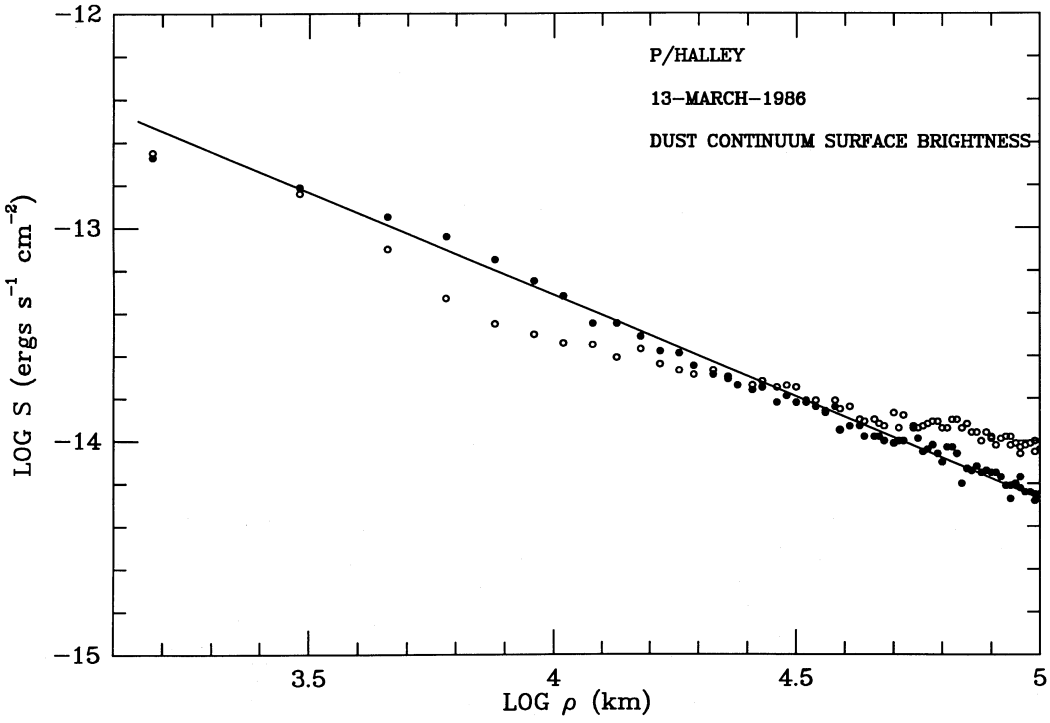

FIG. 10.—Logarithmic surface brightness distribution of the tailward (*open circles*) and Sunward (*filled circles*) dust continuum. Model for ρ^{-1} surface brightness distribution indicated (*solid line*). Note the wave structure, especially in the tailward dust profile.

true for the comet ionosophere where the ions of the most abundant species H_2O and CO are presented in the visible spectrum.

VI. DISCUSSION

The preperihelion ground-based observations of comet Halley indicated an onset of coma formation at $r \approx 6$ AU (Wyckoff *et al.* 1985; Meech, Jewitt, and Ricker 1986), consistent with H_2O models of comet nuclei (Weissman and Kieffer 1981, 1984). Thus it was clear that water controlled the sublimation of frozen gases in comet Halley, as had also been indicated for many years from the nongravitational effects on comet orbits (Marsden, Sekanina, and Yeomans 1973). However, the relative abundances of other ices in comet nuclei have until recently not been determined.

Abundances derived from the *in situ* mass spectrometer data of comet Halley indicate that the coma was composed of $\sim 80\%$ H_2O and $\sim 10\%$ CO with the remaining 10% contributed by trace species, among them those observed in the visible spectral region (Table 4) (Eberhardt *et al.* 1986; Balsiger *et al.* 1986; Ip 1986; Wegmann *et al.* 1987). The ultraviolet *IUE* observations also indicate a dominance of H_2O and CO in the coma (Woods *et al.* 1986). We note that the $Q(H_2O)/Q(CO)$ ratio in comet Halley is close to the clathrate hydrate limit of 6.

Since none of the radicals listed in Table 4 comes directly from photodissociation of H_2O or CO, the observed species must result from (1) fragmentation of other parent molecules, (2) disruption or evaporation of CHON particles (A'Hearn *et al.* 1986*a*; Samarasinha and Klinglesmith 1986; Wallis, Rabilizirov, and Wickramasinghe 1986), or (3) inner coma chemistry (Oppenheimer 1975; Huebner and Giguere 1980).

The parents of the CN and C_2 radicals have long been disputed (see Bockelée-Morvan and Crovisier 1985). The measured production rate of HCN in comet Halley 1986 March 14.1 was 8.2×10^{26} molecules s^{-1} (Schloerb *et al.* 1986), comparable to the observed CN production rate derived here (Table 4). Hence our observations are consistent with CN arising entirely from HCN. However, others have found CN production rates too high for HCN to be the sole source of CN. Moreover, the spatial distribution of CN strongly indicates that a distributed source affected by solar gravitation gives rise to at least part of the observed CN (A'Hearn *et al.* 1986*a*, *b*). It is probable then that the CN arises from a combination of a point and a distributed source.

The production rate ratio for NH_2 relative to H_2O (Table 4) indicates a significantly lower NH_3 abundance than obtained from the spacecraft data. The best estimates from models of the *in situ* data for the abundance ratio, NH_3/H_2O give $\sim 1\%$–2% (Allen 1987; Ip 1986; Wegmann *et al.* 1987). The most likely parent of NH_2 is NH_3 (see Wegmann *et al.* 1987) which for the reaction,

$$NH_3 + h\nu \rightarrow NH_2 + H$$

produces NH_2 with a branching ratio of 95% (Allen 1987). Thus our data indicate that the ammonia abundance ratio in comet Halley was

$$Q(NH_3)/Q(H_2O) \approx Q(NH_2)/[0.95\ Q(H_2O)] \approx 0.3\% .$$

This ratio is ~ 8 times smaller than the NH_3 abundance derived from the *GIOTTO* ion mass spectrometer data by Wegmann *et al.* (1987), and several times lower than that derived by Allen (1987) and colleagues also from an analysis of the *GIOTTO* ions mass spectra. Therefore unless the photodissociation branching ratio for NH_3 is greatly in error, or the dominant source of the observed NH_2 misidentified, there is a significant discrepancy between our computed ammonia abundance and that determined from the spacecraft data. We note that previous ground-based observations of several comets give an abundance ratio, $NH_2/H_2O \approx 0.1\%$ (A'Hearn, Hanisch, and Thurber 1980) corresponding to $NH_3/H_2O \approx 0.1\%$ which indicates that a very low ammonia abundance may be a common property of comets, especially since comet Halley showed relatively strong NH_2 emission compared to other comets observed in recent years.

The models used to calculate the NH_3 abundance from the *GIOTTO* ion mass spectrometer data are quite sensitive to the electron densities which determine the electron recombination rates of the molecular ions (Ip 1985). Because an ambiguity arises at 18 amu where both NH_4^+ and H_2O^+ ions contribute to the ion mass spectrometer count rates, without accurate electron recombination rates it is difficult to model the separate abundances for H_2O^+ and NH_4^+. Fortunately H_2O^+ can be unambiguously identified and its production rate measured from ground-based observations, as will be reported elsewhere (Wyckoff *et al.* 1988).

Unlike the NH_2 spatial profile, our CH observations indicate a multiple or a distributed source, or both. Therefore it is not surprising that the assumption that CH derives solely from CH_4 in the reaction

$$CH_4 + h\nu \rightarrow CH + H_2 + H ,$$

with a branching ratio $\sim 10\%$ (Allen 1987), leads to an abundance ratio CH_4/H_2O several times larger than calculated from the *GIOTTO* ion mass spectra (Allen 1987; Wegmann *et al.* 1987), and twice as large as ground-based limits (Drapatz, Larsen, and Davis 1986). We conclude that the CH observed in the spectrum of comet Halley does not derive predominantly from CH_4. Since hydrocarbons were very abundant in comet Halley (Korth *et al.* 1986), there are many possible additional CH parent molecules. Thus the CH production rate, the CH scale length and the quality of the Haser model fit to the observed CH spatial profile indicate a multiple or a distributed source such as the CHON particles as parents for CH in comet Halley.

The relatively high abundance of CO in comet Halley and the low abundance of NH_3 inferred here reflect the relatively high stability of CO in the gas phase prior to condensation of the nucleus. We note, however, that comet Halley is probably a very evolved comet, with a history of at least 1000 solar passages (Weissman 1985). Therefore the large abundance difference between NH_3 and CO is somewhat puzzling in view of the expected CO depletion by diffusion in successive solar passages as expected on theoretical grounds and from laboratory experiments (see Podolak and Herman 1985). Spacecraft results may provide an explanation for the apparent lack of depletion of CO in comet Halley. Most of the CO observed in this comet arose from a distributed source associated with the CHON particles (Kissel *et al.* 1986) which have been estimated to consist of $\sim 5\%$ (by mass) of H_2CO and $HCO \cdot OH$ (Delsemme 1987). Hence a significant fraction of the CO in comets might be bound in organic compounds trapped in the CHON particles, as suggested by Delsemme (1987). Whether the variations in abundances of the highly volatile gases from comet to comet (see Feldman 1982) are due to the differences in

condensation sites, to subsequently processing in the solid state or to chemical differentiation (Houpis, Ip, and Mendis 1985) will be difficult but important to determine.

We gratefully acknowledge the able assistance of S. Heathcote, M. Navarrate, and E. Cosgrove at the telescope, and the advice of A. Phillips and A. Ferro on IRAF. We also gratefully appreciate the skillful preparation of the manuscript by B. Dunlap. This research was supported in part by NASA grant NAGW-547 to S. W. and P. W.

REFERENCES

A'Hearn, M. F. 1982, in *Comets*, ed. L. L. Wilkening (Tucson: University of Arizona Press), p. 433.
A'Hearn, M. F., Hanisch, R. J., and Thurber, C. H. 1980, *A.J.*, **85**, 74.
A'Hearn, M. F., Hoban, S., Birch, P. V., Bowers, C., Martin, R., and Klinglesmith, III, D. A. 1986*a*, in *Proc. 20th ESLAB Symposium on the Exploration of Halley's Comet, SP-250*, Vol. **1**, ed. B. Battrick, E. J. Rolfe, and R. Reinhard (Paris: ESA), p. 483.
———. 1986*b*, *Nature*, **324**, 649.
Allen, M. A. 1987, private communication.
Bailey, M. E. 1986, *Nature*, **324**, 350.
Balsiger, H., *et al.* 1986, *Nature*, **321**, 330.
Bockelée-Morvan, D., and Crovisier, J. 1985, *Astr. Ap.*, **151**, 90.
Chamberlain, J. W., and Hunten, D. M. 1987, in *Theory of Planetary Atmospheres*, 2d ed., Orlando: Academic Press), p. 290.
Cochran, A. L. 1985, *A.J.*, **90**, 2609.
———. 1987, private communication.
Cochran, A. L., and Barker, E. S. 1986, in *Proc. 20th ESLAB Symposium on the Exploration of Halley's Comet, SP-250*, Vol. **1**, ed. B. Battrick, E. J. Rolfe, and R. Reinhard (Paris: ESA), p. 439.
Combes, M., *et al.* 1986, in *Proc. 20th ESLAB Symposium on the Exploration of Halley's Comet, SP-250*, Vol. **1**, ed. B. Battrick, E. J. Rolfe, and R. Reinhard (Paris: ESA), p. 353.
Combi, M. R., and Delsemme, A. H. 1986, *Ap. J.*, **308**, 472.
Delsemme, A. H. 1982, in *Comets*, ed. L. L. Wilkening (Tucson: University of Arizona Press), p. 85.
———. 1987, preprint.
Delsemme, A. H., and Combi, M. R. 1983, *Ap.J.*, **271**, 388.
Drapatz, S., Larsen, H. P., and Davis, D. S. 1986, in *Proc. 20th ESLAB Symposium on the Exploration Halley's Comet, ESA SP-250*, Vol. **1**, ed. B. Battrick, E. J. Rolfe, and R. Reinhard (Paris: ESA), p. 347.
Eberhardt, P., *et al.* 1986, in *Proc. 20th ESLAB Symposium on the Exploration of Halley's Comet, ESA SP-250*, Vol. **1**, ed. B. Battrick, E. J. Rolfe, and R. Reinhard (Paris: ESA), p. 383.
Feldman, P. D. 1982, in *Comets*, ed. L. L. Wilkening (Tucson: University of Arizona Press), p. 461.
Feldman, P. D., *et al.* 1986, in *Proc. 20th ESLAB Symposium on the Exploration of Halley's Comet, SP-250*, Vol. **1**, ed. B. Battrick, E. J. Rolfe, and R. Reinhard (Paris: ESA), p. 325.
Fernandez, J. A. 1978, *Icarus*, **34**, 173.
———. 1985, in *Dynamics of Comets: Their Origin and Evolution*, ed. A. Carusi and G. B. Valsecchi (Dordrecht: Reidel), p. 45.
Fernandez, J. A., and Ip, W.-H. 1981, *Icarus*, **47**, 470.
———. 1983, *Icarus*, **54**, 377.
Festou, M. C. 1981, *Astr. Ap.*, **95**, 69.
Gredel, R. 1987, prviate communication.
Haser, L. 1957, *Bull. Acad. Roy. de Belgique, Classe des sci., 5th ser.*, **43**, 740.
Hayward, T. L., Gehrz, R. D., and Grasdalen, G. L. 1987, *Nature*, **326**, 55.
Heisler, J., and Tremaine, S. 1986, *Icarus*, **65**, 13.
Houpis, H. L. F., and Gombosi, T. I. 1986, in *Proc. 20th ESLAB Symposium on the Exploration of Halley's Comet, SP-250*, Vol. **2**, ed. B. Battrick, E. J. Rolfe, and R. Reinhard (Paris: ESA), p. 397.
Houpis, H. L. F., Ip, W.-H., and Mendis, D. A. 1985, *Ap. J.*, **295**, 654.
Huebner, W. F., and Giguere, P. T. 1980, *Ap. J.*, **238**, 753.
Ip, W.-H. 1985, *Adv. Space Res.*, **5**, No. 12, 233.
Ip, W.-H. 1987, private communication.
Kissel, J., *et al.* 1986*a*, *Nature*, **321**, 280.
———. 1986*b*, *Nature*, **321**, 336.
Korth, A., *et al.* 1986, *Nature*, **321**, 335.
Krankowsky, D., *et al.* 1986, *Nature*, **321**, 326.
Larson, H. P., Davis, D. S., Mumma, M. J., and Weaver, H. A. 1986, in *Proc. 20th ESLAB Symposium on the Exploration of Halley's Comet, SP-250*, Vol. **1**, ed. B. Battrick, E. J. Rolfe, and R. Reinhard (Paris: ESA), p. 335.
Marsden, B. G., Sekanina, Z., and Yeomans, D. K. 1973, *A.J.*, **78**, 211.
Meech, K. J., Jewitt, D., and Ricker, G. R. 1986, *Icarus*, **66**, 561.
Mumma, M. J., Weaver, H. A., and Larson, H. P. 1986, in *Proc. 20th ESLAB Symposium on the Exploration of Halley's Comet, SP-250*, Vol. **1**, ed. B. Battrick, E. J. Rolfe, and R. Reinhard (Paris: ESA), p. 341.
Newburn, R. L., and Spinrad, H. 1984, *A.J.*, **89**, 289.
O'Dell, C. R., and Osterbrock, D. E. 1962, *Ap. J.*, **136**, 559.
Oort, J. H. 1950, *Bull. Astr. Netherlands*, **11**, No. 408, 91.
Oppenheimer, M. 1975, *Ap. J.*, **196**, 251.
Podolak, M., and Herman, G. 1985, *Icarus*, **61**, 267.
Samarasinha, N. H., and Klinglesmith III, D. A. 1986, in *Proc. 20th ESLAB Symposium on the Exploration of Halley's Comet, SP-250*, Vol. **1**, ed. B. Battrick, E. J. Rolfe, and R. Reinhard (Paris: ESA), p. 487.
Schleicher, D. 1981, Ph.D. thesis, University of Maryland.
Schloerb, F. P., Kinzel, W. M., Swade, D. A., and Irvine, W. M. 1986, in *Proc. 20th ESLAB Symposium on the Exploration of Halley's Comet, SP-250*, Vol. **1**, ed. B. Battrick, E. J. Rolfe, and R. Reinhard (Paris: ESA), p. 577.
Scoville, N. Z., and Saunders, D. B. 1986, in *The Galaxy and the Solar System*, ed. R. Smoluchowski, J. N. Bahcall, and M. S. Matthews (Tucson: University of Arizona Press), p. 69.
Singh, P. D., and Dalgarno, A. 1987, in *ESA Symposium on the Diversity and Similarities among Comets, SP-278*, ed. B. Battrick and E. J. Rolfe (Paris: ESA), (in press).
Spinrad, H. 1987, *Ann. Rev. Astr. Ap.*, **25**, 231.
Stone, R., and Baldwin, J. 1983, *M.N.R.A.S.*, **204**, 347.
Swings, P. 1941, *Lick Obs. Bull.*, **19**, No. 408, 131.
Thaddeus, P. 1986, in *The Galaxy and the Solar System*, ed. R. Smoluchowski, J. N. Bahcall, and M. S. Matthews (Tucson: University of Arizona Press), p. 61.
Torbett, M. V. 1986, in *The Galaxy and the Solar System*, ed. R. Smoluchowski, J. N. Bahcall, and M. S. Matthews (Tucson: University of Arizona Press), p. 147.
Wallis, M. K., Rabilizirov, R., and Wickramasinghe, N. C. 1986, in *Proc. 20th ESLAB Symposium on the Exploration of Halley's Comet, SP-250*, Vol. **2**, ed. B. Battrick, E. J. Rolfe, and R. Reinhard (Paris: ESA), p. 251.
Wegmann, R., Schmidt, H. U., Huebner, W. F., and Boice, D. C. 1987, *Astr. Ap.*, in press.
Weissman, P. R. 1985, *Space Science Rev.*, **41**, 299.
Weissman, P. R., and Kieffer, H. H. 1981, *Icarus*, **47**, 302.
———. 1984, *J. Geophys. Res.*, **89**, 358.
Woods, T. N., Feldman, P. D., and Dymond, K. F. 1986, in *Proc. 20th ESLAB Symposium on the Exploration of Halley's Comet, SP-250*, Vol. **1**, ed. B. Battrick, E. J. Rolfe, and R. Reinhard (Paris: ESA), p. 431.
Wyckoff, S., *et al.* 1988, in preparation.
Wyckoff, S., Wagner, R. M., Wehinger, P. A., Schleicher, D. G., and Festou, M. C. 1985, *Nature*, **316**, 241.

MICHAEL J. S. BELTON: National Optical Astronomy Observatories, P.O. Box 26732, Tucson, AZ 85726

HYRON SPINRAD: Astronomy Department, University of California, Berkeley, CA 94720

STEPHEN TEGLER, PETER A. WEHINGER, and SUSAN WYCKOFF: Department of Physics, Arizona State University, Tempe, AZ 85287